Carbon 232 (2025) 119799

Contents lists available at ScienceDirect

Carbon

journal homepage: www.elsevier.com/locate/carbon

Electrochemical reduction and recovery of trace gold(I) from environmentally friendly thiosulfate leaching solutions using carbon electrodes

Qizheng Weng [a,b], Weiquan Zhan [c,d,*], Xuan Zhang [a], Shaoxian Song [e], Zhenlong Zeng [b], Hnin May Lwin [f], José Luis Arauz-Lara [c], Feifei Jia [a,b,**]

[a] Key Laboratory of Green Utilization of Critical Non-metallic Mineral Resources of Ministry of Education, Wuhan, 430070, Hubei, China
[b] School of Resources and Environmental Engineering, Wuhan University of Technology, Wenzhi Street 34, Wuhan, 430070, Hubei, China
[c] Instituto de Física, Universidad Autónoma de San Luis Potosí, Av. Manuel Nava 6, Zona Universitaria, San Luis Potosí, 78290, Mexico
[d] Department of Mining and Minerals Engineering, Virginia Polytechnic Institute and State University, Blacksburg, VA, 24061, United States
[e] Instituto de Metalurgia, Universidad Autónoma de San Luis Potosí, Av. Sierra Leona 550, San Luis Potosí, 78210, Mexico
[f] Department of Industrial Chemistry, West Yangon University, Myanmar

ARTICLE INFO

Keywords:
Electro reduction-recovery
Trace $Au(S_2O_3)_2^{3-}$
Carbon electrodes
Au^0

ABSTRACT

Efficient recovery of $Au(S_2O_3)_2^{3-}$ at low concentrations is a key challenge for the development of environmentally friendly, cyanide-free thiosulfate leaching methods in industry. In the study, carbon materials including activated carbon (AC), graphite, and graphene were used as electrodes for electrochemical reduction and recovery (electro reduction-recovery) of trace gold(I) from thiosulfate leaching solutions ($Au(S_2O_3)_2^{3-}$). The results demonstrated that $Au(S_2O_3)_2^{3-}$ could be efficiently recovered in the form of Au^0 with nearly 100 % recovery from both simulated and actual gold ore leaching solutions, significantly simplifying traditional recovery and reduction processes. Even in the presence of impurities such as cations and $S_2O_3^{2-}$, recovery remained high, around 90 %. Among the parameters studied, applied voltage was the most critical for optimizing recovery, as it enhanced ion migration and significantly improved gold reduction. The study investigated the relationship between the intrinsic properties of carbon materials and their electrochemical reduction and recovery capabilities. Rich porosity of carbon materials promoted interactions with $Au(S_2O_3)_2^{3-}$, enhancing the electric double layer capacity, while π–π* satellite transitions played a dominant role in the charge transfer, thereby improving the reduction rate. This research offers new insights of the mechanisms behind the recovery of trace $Au(S_2O_3)_2^{3-}$ from thiosulfate leaching solutions through carbon electrodes.

1. Introduction

Gold, an essential metal resource [1,2], faces substantial extraction challenges due to the limitations of conventional cyanide leaching, which is increasingly criticized for its environmental impact and inefficiency in processing low-grade ores [3]. Thiosulfate leaching has emerged as a more environmentally friendly, cyanide-free alternative for gold extraction[4–6], even from refractory ores [7]. However, despite its potential, this method has not seen widespread industrial application owing to inefficiencies in recovering gold thiosulfate ions ($Au(S_2O_3)_2^{3-}$) at low concentrations.

Extensive research has explored various recovery methods, including precipitation [8], solvent extraction [9], adsorption [10], and electrodeposition [11], yet significant challenges remain under real-world low-concentration conditions. These challenges primarily stem from two key factors: weak interactions between $Au(S_2O_3)_2^{3-}$ and adsorbents, attribute to the ion's large molecular weight and the complex leaching solutions. Another concern involves the low purity and high costs associated with certain recovery techniques like chemical precipitation [12,13] and ion-exchange [14,15]. Given these issues, developing efficient and cost-effective methods for recovering $Au(S_2O_3)_2^{3-}$ from thiosulfate leaching solutions is crucial. Addressing the limitations in existing methods, particularly under low-concentration conditions, remains a critical area of research in hydrometallurgy, with the goal of

* Corresponding author. Instituto de Física, Universidad Autónoma de San Luis Potosí, Av. Manuel Nava 6, Zona Universitaria, San Luis Potosí, 78290, Mexico.
** Corresponding author. Key Laboratory of Green Utilization of Critical Non-metallic Mineral Resources of Ministry of Education, Wuhan, 430070, Hubei, China.
E-mail addresses: zhan_weiquan@163.com (W. Zhan), feifeijia@whut.edu.cn (F. Jia).

https://doi.org/10.1016/j.carbon.2024.119799
Received 29 August 2024; Received in revised form 23 October 2024; Accepted 2 November 2024
Available online 4 November 2024

enabling more sustainable and economically viable gold extraction processes.

Catalytic reduction-recovery based on molybdenum disulfide was proposed in our previous works to realizing adsorption and reduction together [16–18], which shortened the traditional gold extraction procedures, while it was hard in selectively recovering $Au(S_2O_3)_2^{3-}$ in actual leaching solutions. In the thiosulfate leaching solutions, mole ratio of $S_2O_3^{2-}$ and $Au(S_2O_3)_2^{3-}$ was higher than 3:1, causing a great obstacle to low-concentration $Au(S_2O_3)_2^{3-}$ recovery. According to the electrochemical theory [19], large and small amounts of ions migrate differently under an external field. Our recent researches have proved that Au $(S_2O_3)_2^{3-}$ can be separated and recovered with an applied voltage [20]. The choice of materials used as electrodes for electro reduction-recovery is crucial for the recovery of $Au(S_2O_3)_2^{3-}$.

Based on the electric double layer capacity property, rich porous structure of electrodes with high surface area is beneficial for ions storage and reaction [21,22]. In addition to its electrochemical reduction properties, when the applied voltage exceeds a certain threshold (0.25 V) [23], $Au(S_2O_3)_2^{3-}$ can be reduced into gold metal, achieving both adsorption and reduction simultaneously. Carbon materials such as activated carbon (AC), graphite, graphene, and carbon nanotubes, known for their super porous structure, are widely employed as electrodes in various applications including desalination [24,25],batteries [26–28], and metals adsorption [29–31]. Leveraging its porous material structure of carbon materials, this method enables the efficient recovery of low concentration $Au(S_2O_3)_2^{3-}$ at a low cost, while also facilitating simultaneous reduction. However, few works focus on the electro reduction-recovery of $Au(S_2O_3)_2^{3-}$ based on carbon electrodes and relevant reaction mechanism.

Here, AC, graphene, and graphite were selected as carbon electrodes to investigate the electro reduction-recovery of $Au(S_2O_3)_2^{3-}$. The porous structure and functional groups of carbon materials were thoroughly researched, along with their impact on the recovery performances of Au $(S_2O_3)_2^{3-}$. The study aims to comprehensively explore and utilize carbon materials for electro reduction-recovery of $Au(S_2O_3)_2^{3-}$, thereby advancing the application of thiosulfate leaching in the gold industries.

2. Experimental

2.1. Materials

Ammonium thiosulfate ($(NH_4)_2S_2O_3$, 98 wt%) was purchased from Sigma-Aldrich (Shanghai, China). Standard chloroauric acid ($HAuCl_4$, 1000 mg L^{-1}) was obtained from Well Group Scientific Ltd., USA. High pure flake graphite (99 wt%) was the product from XFNANO, Jiangsu, China. Graphite powder (Graphite) was got from Shanghai Macklin Biochemical Technology Co., Ltd. Sodium hydroxide (NaOH), sodium sulfate (Na_2SO_4), charcoal activated powder (AC), potassium permanganate ($KMnO_4$), sulfuric acid (H_2SO_4), hydrazine hydrate ($N_2H_4{\cdot}H_2O$), calcium chloride ($CaCl_2$), magnesium chloride ($MgCl_2$), aluminium chloride ($AlCl_3$), ferrous chloride ($FeCl_2$), lead chloride ($PbCl_2$), cupric chloride ($CuCl_2$), nickel chloride ($NiCl_2$), manganous chloride ($MnCl_2$), sodium thiosulfate ($Na_2S_2O_3$), sodium sulfite (Na_2SO_3), copper sulfate pentahydrate ($CuSO_4{\cdot}5H_2O$), 5 % ammonia solution ($NH_3{\cdot}H_2O$) and dimethylacetamide (DMA) (12.5 mg mL^{-1}) were bought from Sinopharm Chemical Reagent Co., Ltd. (Shanghai, China). Vinylidene fluoride ($C_2H_2F_2$) was procured from Alfa Aesar (China) Chemicals Co., Ltd. Conductive carbon black was obtained from American Cabot, while carbon black was acquired from Suzhou Sinero Technology Co., Ltd. (China). Deionized water was produced by Millipore SAS (France) with 18.2 MΩ cm. Pt plate and Hg/HgO reference electrode were bought from SHANGHAI CHUXI INDUSTRIAL CO., LTD.

2.2. Characterizations

X-ray diffraction (XRD, D8 Advance, Bruker AXS, Germany) with Cu-Kα radiation was used to analyze the internal structure and morphology of materials. Raman spectra was obtained utilizing an INVIA Raman microscope with an Ar laser (Renishaw, England). The American Thermo Scientific Nicolet 6700 was used for analyzing materials' surface functional groups in the wavenumber range of 4000–400 cm^{-1}. The Brunauer–Emmett–Teller method (BET, V-Sorb X800, China) was employed to investigate the pore structure distribution, adsorption and desorption isotherms. Microstructures were obtained via scanning electron microscope (SEM, Phenom ProX G6, Netherlands). The chemical element state was determined by X-ray photoelectron spectroscopy (XPS, Thermo Scientific K-Alpha, America). The Agilent 280FS AA Spectrometer (G8434A, America) was used to determine the gold concentration of the filtrate.

2.3. Preparation of graphene

Graphene was prepared by oxidation-reduction method. Initially, graphene oxide was prepared from graphite powder, which was subsequently reduced to obtain graphene. In a controlled environment, 5 g of graphite powder was mixed with 115 mL of 98 % concentrated sulfuric acid in an ice bath and stirred for 30 min. Then, 20 g $KMnO_4$ was added to the mixture, and the stirring continued for an additional hour. The mixture was transferred to a warm water bath at 40 °C, where stirring continued for another 30 min. Afterward, distilled water was gradually added to dilute the reaction solution to a total volume of 800 mL, ensuring that the temperature remained below 100 °C. An appropriate amount of H_2O_2 was added until the solution turned yellow. The mixture was then centrifuged while hot, washed with 5 % HCl and distilled water until near neutral, and finally filtered. The resulting graphene oxide was washed and dried at 60 °C.

The synthesis of graphene was achieved through the reduction of graphene oxide, as outlined below. Graphene oxide dispersion was prepared by weighing 0.1 g graphite oxide and adding it to 200 mL of NaOH solution with pH = 11, and being ultrasonicated at 150 W for 90 min. Afterward, the dispersion was centrifuged at 4000 r·min^{-1} for 3 min to remove the residual graphite oxide. 0.2 mL of hydrazine hydrate was added to the centrifuged graphene oxide dispersion, and the graphene suspension was obtained by reacting at 90 °C for 2 h. The graphene suspension was sealed and left to stand for a few days to observe its dispersion effect. After confirming the suspension was ideal, it was filtered and lyophilized to gain graphene.

2.4. Fabrication of carbon electrodes

Conductive carbon black functions to enhance electrode conductivity, improve cycling stability, increase electrochemical activity [32]. Polyvinylidene fluoride, as a traditional binder, provides firmness, stability, good thermal stability, and a high dielectric constant. AC (or graphite or graphene), conductive carbon black and polyvinylidene fluoride were evenly mixed in a mortar at a mass ratio of 8:1:1 and dissolved in DMA. Titanium plate with anti-corrosion[33–35], wide-application was chosen as substrate for coating carbon materials. Approximately 30 ± 5 mg of the mixture was then evenly coated onto the Ti plate using the flat part on the back of the spoon. The electrode was then heated at 60 °C for at least 1 h to remove the residual organic solvent. Finally, the electrode was immersed in deionized water and allowed to soak until ready for use.

2.5. Electro reduction-recovery of $Au(S_2O_3)_2^{3-}$

The ammonium thiosulfate was prepared with deionized water with the molar ratio of Au to $S_2O_3^{2-}$ as 1 to 4. Chloroauric acid and sodium hydroxide were added drop by drop to keep the pH of the solution at 10.

A pair of carbon electrodes was put at 5 mm distance into the electrolytic cell that contained $Au(S_2O_3)_2^{3-}$ with external voltage (1.2 V). The cell was connected to a peristaltic pump with a speed of 50 r/min.

2.5 mL of solution would be extracted and filtered using a 0.22 μm filter membrane at 0, 1, 2, 4, 7, 10, and 22 h. The concentration of filtrate was determined by the atomic absorption spectrometer. The following formulas were used for calculating the reduction (*Re*) and recovery (*R*):

$$R_e = \frac{(C_0 - C_t) \times (V_0 - V_t)}{m} \quad (1)$$

$$R = \frac{(C_0 - C_t)}{C_0} \times 100\% \quad (2)$$

where C_0 and C_t are the concentrations of Au at the initial and time *t*, respectively, mg·L^{-1}; V_0 and V_t are the volumes of reaction solution at the initial and time *t*, respectively, L; and m is the material mass used in the electrode, mg.

2.6. Thiosulfate leaching in gold ores

The gold ores (China) were mixed evenly by pile cone and then leached by copper–sodium thiosulfate system. System (0.3 M $Na_2S_2O_3$, Na_2SO_3, $CuSO_4{\cdot}5H_2O$, 5 % $NH_3{\cdot}H_2O$) with the pH of 10 and the leaching time of 12 h were used to leaching the gold ores. As a leaching agent, $Na_2S_2O_3$ had the capacity to facilitate the dissolution of gold. The use of Na_2SO_3 could reduce the consumption of thiosulfate. Firstly, sulfites possess reducibility, which could diminish the oxidation-reduction potential of the overall solution, thereby reducing the consumption of thiosulfate and enhancing the stability of thiosulfate. Second, the thiosulfate ion was unstable in solution and would decompose. One of the decomposition products was sulfite, and the addition of sulfite can prevent the reaction, thereby reducing the effect of thiosulfate consumption. The oxidizing agent Cu^{2+} in $CuSO_4{\cdot}5H_2O$ could catalyze leaching, promote the dissolution of gold and oxidize $S_2O_3^{2-}$. While the dissolution of gold can be accelerated by $NH_3{\cdot}H_2O$, which in turn facilitated the stabilization of thiosulfate ions and the maintenance of solution pH. Furthermore, ammonia formed complexes with copper ions, which also facilitate the dissolution of gold. The leachate was decanted and stored for subsequent use.

2.7. Electrochemical measurements

Electrochemical impedance spectroscopy (EIS) and cyclic voltammetry (CV) were run on VersaSTAT-450, PAR, USA. A three-electrode system was used for both experiments in 50 mL of 1 mol L^{-1} Na_2SO_4 and 5 mg L^{-1} $Au(S_2O_3)_2^{3-}$. A Pt plate and a Hg/HgO 1 M KOH electrode were used as counter and reference electrodes, respectively. The working electrode of approximately 1 cm^2 operated in this process was made from the same material as the electrode used in the Au removal experiment. The frequency range of the EIS test was 0.01–10000 Hz. The following formula was used for calculating the specific capacitance (*C*):

$$C = \frac{\int IdV}{2mv\Delta V} \quad (3)$$

where *C* is the specific capacitance, F·g^{-1}; *I* is the discharge current, A; m is the mass of material on working electrode, g^{-1}; *v* is the scan rate, mV·s^{-1}; and ΔV is the working voltage window, V.

3. Results and discussion

3.1. Structure characterization

Microstructure of AC, graphite, and graphene were characterized by X-ray diffraction (XRD). X-ray photoelectron spectroscopy (XPS), Raman, and Fourier transform infrared spectroscopy (FTIR) were used to observe functional groups. In Fig. 1(a), AC had only two broad peaks at about 25°and 43°, an indication that it had an amorphous structure. Upward warping at a low diffraction angle in AC was ascribed to high porosity [36]. The peaks in graphene resemble those in AC, with the difference being a broader and smoother shape, indicating lower porosity in graphene. Unlike the two materials above, graphite had two distinct peaks, one clear characteristic peak at 26.5° corresponding to the (002) crystallographic plane of the graphite structure. The sharp peak pattern indicated a high degree of graphite crystallization. Another peak at 54.5° of (004) facet could be used to evaluate the degree of graphitization, that was the degree to which carbon atoms form a

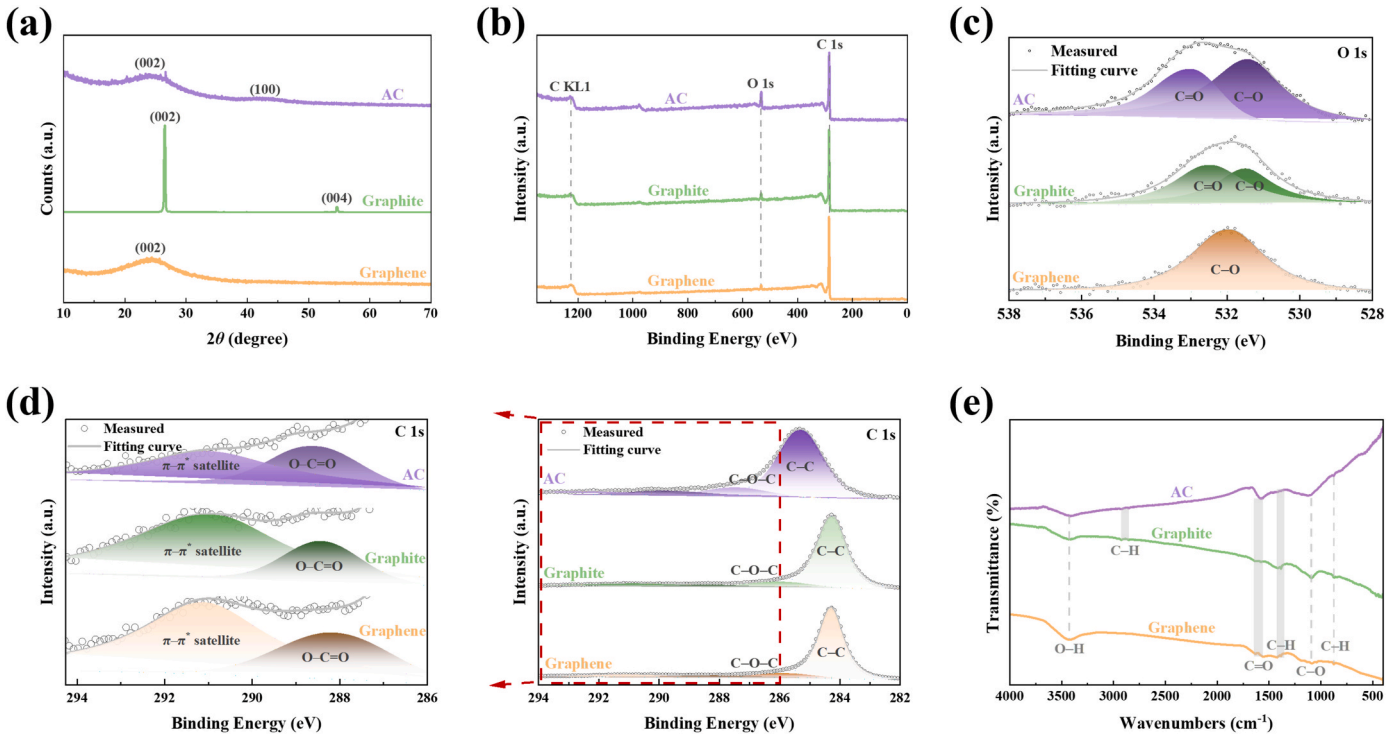

Fig. 1. (a) XRD patterns, XPS (b) survey spectra, (c) O 1s spectra, (d) C 1s spectra, and (e) FTIR patterns of carbon materials.

densely packed hexagonal graphite crystal structure [37]. The sharp peak here meant the degree of graphitization was high. All the results indicated that the carbon materials exhibit high purity.

XPS had been used to investigate the chemical states of elements in carbon materials. In Fig. 1(b), there were strong absorption peaks at binding energies of 1229, 532, and 284 eV in the survey spectrum, belonging to the absorption peaks of C KL1, O 1s, and C 1s, respectively, which indicated that the C and O elements were the main constituents in the three carbon materials. Fig. 1(c) displayed the O 1s XPS spectrum, and the fitted peaks at about 531 and 533 eV were raised from C–O and C═O groups, respectively, while there was only C–O peak in graphene might due to the small number of other groups. To further study the group information, C 1s XPS spectrum was given in Fig. 1(d). Binding energy peaks at about 284, 286, 288, and 290 eV in carbon materials were corresponded to the C–C, C–O–C, O–C═O, and π–π* satellite, respectively [38]. To elucidate the role of functional groups, the carbon material's composition from C 1s analysis was presented, as shown in Table 1. Among the three materials, graphene exhibited the highest proportion of π–π* satellite, indicating that the conjugated π-electron system of graphene was more continuous and ordered, and electrons could move more freely in the material. This also signified that it exhibited the highest electron mobility. Furthermore, graphene exhibited the highest proportion of oxygen functional groups among all carbon materials, which could enhance its interaction with $Au(S_2O_3)_2^{3-}$.

Aiming to further investigate more functional groups of the three materials, FTIR was performed and the results were shown in Fig. 1(e). The peaks at about 3420, 3922, 2850, 1638, 1560, 1420, 1380, 1100 and 874 cm^{-1} were attributed to the stretching vibration of O–H, C–H, C–H, C═O, C═O, C–H, C–H, C–O and C–H, respectively, which could be seen in the three materials [39]. As for the peak at 2925–2850 cm^{-1} ascribed to C–H, it was only found in AC and graphite. Anyways, the three materials were very similar in terms of elemental composition and functional groupings.

The degree of graphitization had a negligible effect on the properties of carbon materials. Despite the high degree of graphitization observed in graphene, the recovery was found to be lower than that of AC, indicating that the effect of graphitization was not particularly pronounced. As evidenced by prior research, oxygen-containing functional groups exert a pronounced influence on the adsorption of $Au(S_2O_3)_2^{3-}$ [40,41]. Nevertheless, the three carbon materials under consideration in this study, as evidenced by the results of FTIR and XPS analyses, exhibited comparable oxygen-containing functional groups. Accordingly, the discrepancy in the recovery observed in this study can be attributed primarily to variations in surface area and aperture.

3.2. Morphology and pore characteristics

The morphology of carbon materials was characterized by scanning electron microscope (SEM). From Fig. 2(a–c) it was obvious that among the three carbon materials, graphite had the largest size, followed by AC. The surface of AC was relatively rough with visible pores, while graphite surface was smooth and hard, and graphene was soft and stackable. Accordingly, peaks for elemental C and O were found in insert picture in Fig. 2(d–f), which indicated that the existence of C and O. The atomic concentration was further provided, and O concentration in graphene was highest, that in AC took second. The discovered patterns were consistent with the oxygen group content observed in XPS.

The characteristics of pores was explored using the BET method. The N_2 adsorption–desorption curves were shown in Fig. 3(a). AC exhibited a type IV isotherm with an H4 hysteresis loop in the vicinity of high pressure, indicating that it was a material with a mixed structure of micropores and mesopores, containing a solid with narrow crack pores. Graphite and graphene belonged to the type IV isotherms with H3 hysteresis loops, which indicated that graphite and graphene were mainly materials with a layered structure. Based on the curves, the specific surface areas of materials were given in Fig. 3(b). It showed that the specific surface area of graphite was very small, indicating that its pore structure was not well developed. Compared to the others, graphene had a larger specific surface area. Among the three materials, AC has the largest specific surface area, mainly due to the abundance of micropores and mesopores.

Furthermore, the pore structure of materials was obtained, and the cumulative pore volume curves were shown in Fig. 3(c). It can be concluded that the pore volume of AC was mainly provided by mesopores, while the pore volume of graphene was mainly provided by macropores. The cumulative pore volume of graphite was very small and mainly provided by macropores. The aperture distribution diagram was shown in Fig. 3(d). It could be seen that AC was predominantly mesoporous, with micropores and a small amount of macropores. Graphite had no micropores, but has trace mesopores and trace macropores. And graphene had very small amounts of micropores, mainly mesopores, and the pore volume provided by macropores and mesopores did not have significantly disparity. It could be calculated that the porosity of AC was the highest, and graphite was the lowest. The size rule was consistent with the porosity when considering the specific surface area. As the porosity increased, the specific surface area also increased, thereby expanding the reaction sites and improving the recovery. While, the available test results indicated that there were no significant differences in the functional groups among the three materials. Instead, the primary distinction was in their structural composition. It can be concluded that the electrochemical effect and recovery were enhanced with an increase in pores and specific surface area.

Table 1
Proportion of functional groups in carbon materials.

	π–π* satellite	O–C═O	C–O–C
AC	10.28 %	6.41 %	9.88 %
Graphite	9.49 %	3.98 %	8.26 %
Graphene	14.88 %	7.72 %	15.03 %

3.3. Electro reduction-recovery performances

$Au(S_2O_3)_2^{3-}$ recovery performances by the electrode made from different carbon materials were evaluated. The adsorption capacity and corresponding recovery of different electrode materials were shown in Fig. 4. As shown in the figure, the bar chart and the line with data points represented reduction and recovery, respectively. The double coordinate diagrams following were also the same. At a concentration of 1 mg L^{-1} $Au(S_2O_3)_2^{3-}$, the order of recovery ability from high to low was by AC, graphene, graphite and finally titanium plate electrodes. In Fig. 4 (a), AC electrodes had the highest recovery among the three materials, reaching 100 %, followed by graphene electrodes at 79 %. While, graphite electrodes had the lowest recovery which reached 68 %. AC electrodes' highest recovery presumably due to its rich pore structure. Compared to graphite electrodes, graphene electrodes had more pores, which may be the main reason for its higher recovery. It was obvious that titanium plate showed a very low recovery as shown in Fig. 4(b), primarily as a substrate in the electro reduction-recovery process. The results of recovery confirming that low-concentration $Au(S_2O_3)_2^{3-}$ can be efficiently recovered by electroreduction.

Moreover, the effects of environmental solutions and operational parameters including concentration, pH, electrodes-spacing, and applied voltage on $Au(S_2O_3)_2^{3-}$ recovery were considered. The recovery performances under different initial gold(I) concentrations (0.1, 0.5, 1, 2, 5, 7, 10, 20, and 50 mg L^{-1}) were shown in Fig. 5(a). Within the gold (I) concentration range of 0.1–50 mg L^{-1}, carbon electrodes exhibited excellent recovery and adsorption capacity of $Au(S_2O_3)_2^{3-}$, confirming that low concentration $Au(S_2O_3)_2^{3-}$ could be recovered by electro reduction-recovery method. Under the concentrations of 20 and 50 mg L^{-1}, the method could still achieve a recovery of more than 90 %. If the recovery needs to be further improved, the number of plates can be

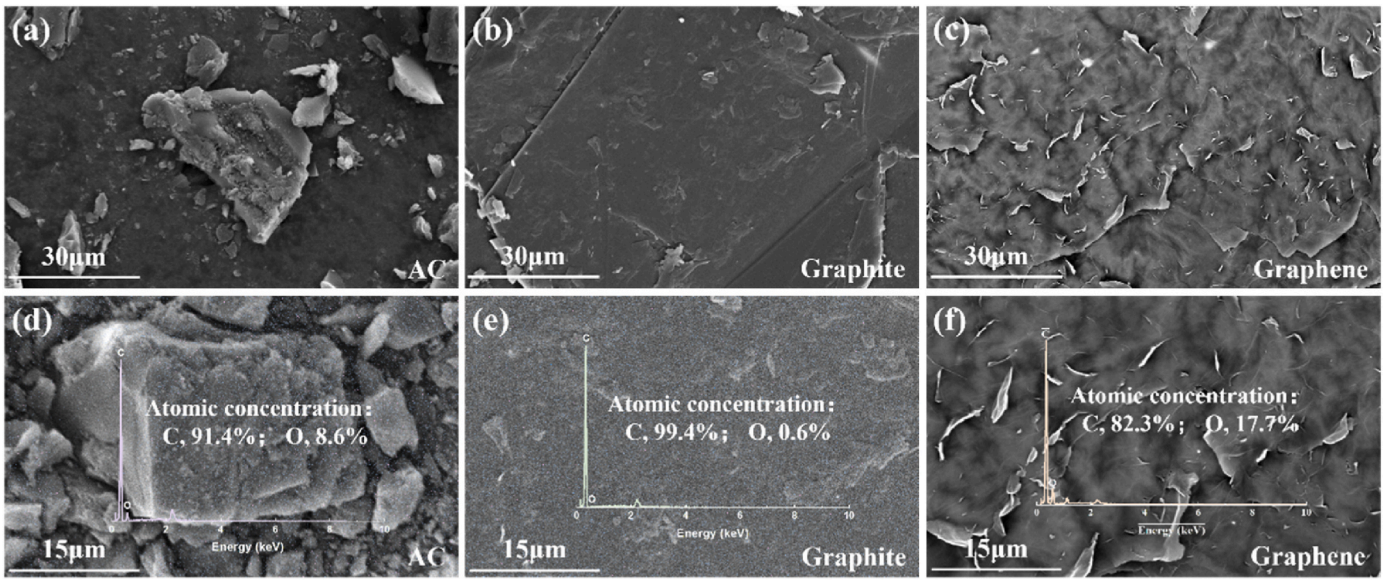

Fig. 2. SEM images of (a, d) AC, (b, e) graphite, and (c, f) graphene.

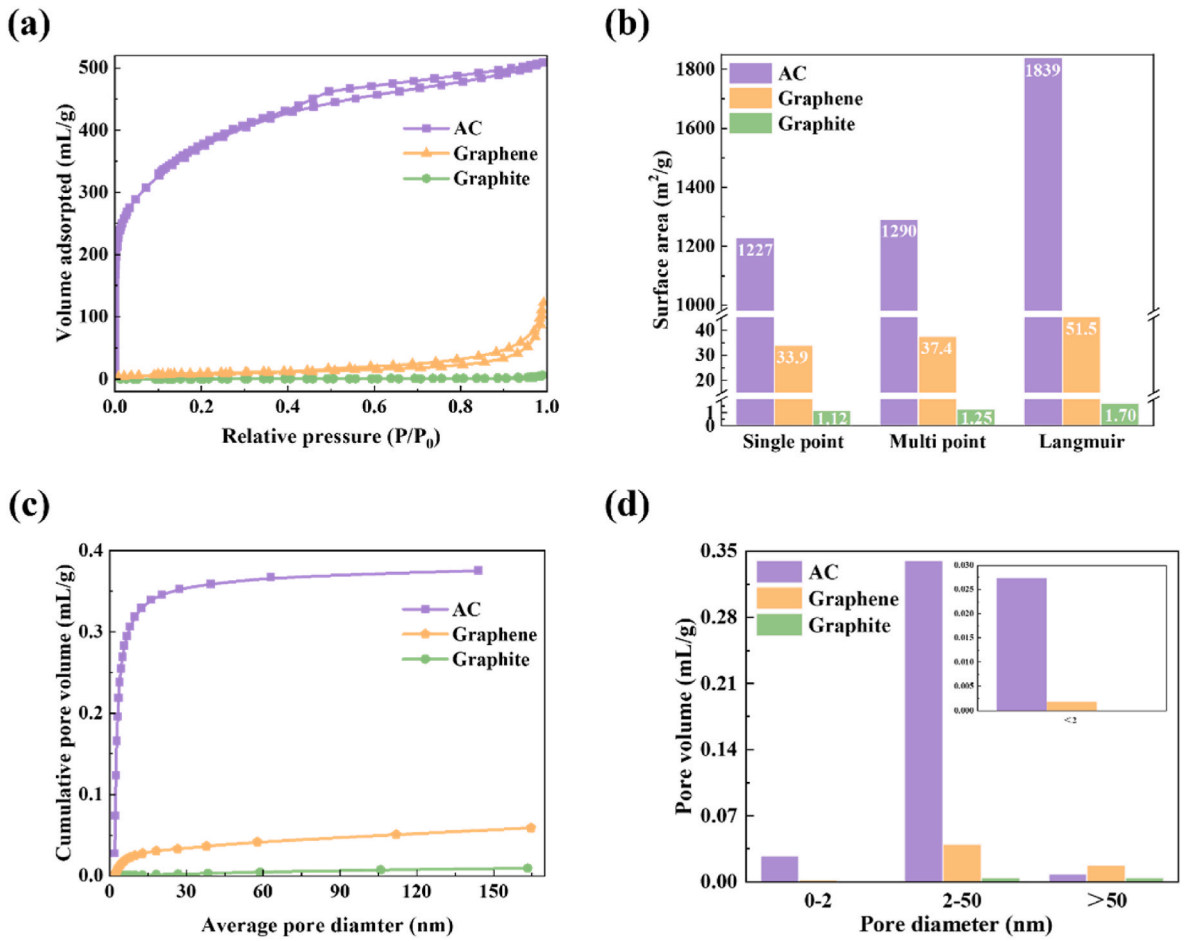

Fig. 3. (a) Nitrogen adsorption–desorption isotherms, (b) specific surface area, (c) cumulative pore volume curves, and (d) pore size distribution of carbon materials.

increased, which was also used in industry. Given that $Au(S_2O_3)_2^{3-}$ is stable in alkaline conditions, the pH of the solution was examined between 8 and 12 (Fig. 5(b)). It was evident that the recovery remained high until 10, at which point it declined due to the increased competition from the ion OH^- for reactive sites [42]. Fig. 5(c) depicted the reduction performances at varying electrodes-spacings, with the optimal recovery effect observed at 5 mm. It can be postulated that when the distance between the plates was minimal, the convection of the solution between the two electrodes would be reduced, which in turn resulted in a decline in the recovery. Conversely, when the distance between the

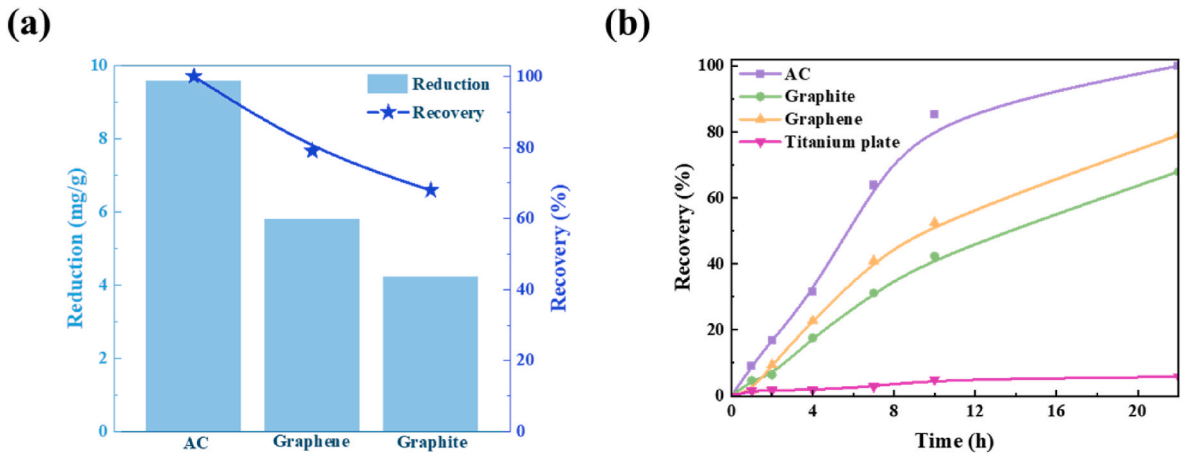

Fig. 4. $Au(S_2O_3)_2^{3-}$ recovery performances of (a) various carbon electrodes, and (b) the variation of recovery over time by with and without carbon materials coating.

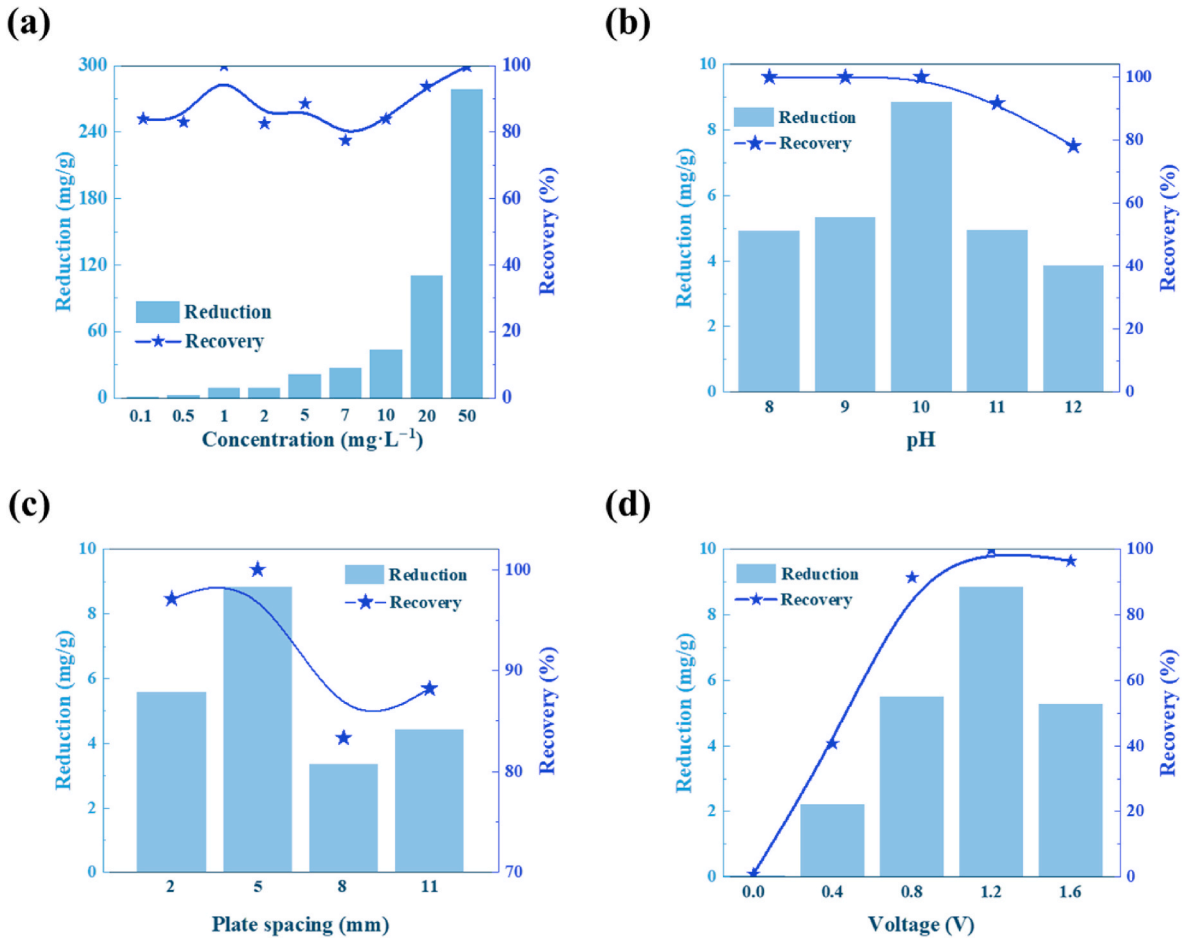

Fig. 5. $Au(S_2O_3)_2^{3-}$ recovery performances by carbon electrodes under different environmental conditions: (a) concentration, (b) pH, (c) electrodes-spacing, (d) applied voltage.

plates was considerable, the influence of electric field force on the recovery of gold was reduced. The applied voltage represented a pivotal parameter in the recovery process of $Au(S_2O_3)_2^{3-}$ (Fig. 5(d)). In the absence of an applied voltage, the recovery of $Au(S_2O_3)_2^{3-}$ was markedly inferior. Following the application of a voltage to the electrode, $Au(S_2O_3)_2^{3-}$ migrated within the solution, with the recovery increasing in accordance with the magnitude of the applied voltage. When the voltage reached a sufficient level, the influence of electrostatic interactions overcame that of volume repulsion, and ions began to accumulate in the pores. The accumulation of ions in the pores resulted in the formation of surface charges on the porous electrode. The enhanced surface charges attracted a greater number of ions into the pores, thereby significantly enhancing the recovery. Furthermore, the correlation was calculated based on the recovery results. As illustrated in Fig. S1, voltage represented the most critical parameter for optimizing the recovery, as it enhanced ion migration and significantly improved the recovery. In

addition, the recovery of graphite and graphene at different concentrations(2, 5, 10 mg L^{-1}) was also evaluated in Fig. S2.

3.4. $Au(S_2O_3)_2^{3-}$ recovery from leaching solutions

To evaluate the application of electro reduction-recovery by carbon electrodes in $Au(S_2O_3)_2^{3-}$ recovery, elemental components in gold ore leaching solutions was tested by ICP (Fig. S3), and recovery performances in the presence of inferred ions were studied (Fig. 6(a)). In the presence of impurity ions, among which, except for Mn^{2+}, the Au $(S_2O_3)_2^{3-}$ recovery reached over 90 %, while only reached 83 % when Mn^{2+} existed. The reason for this might be that under the condition of pH = 10, Mn^{2+} was the least likely to precipitate. The hydrated ions of manganese were relatively stable under alkaline conditions, and the tendency to form precipitates was not as significant as that of other metal ions [43], which in fact influenced the recovery of $Au(S_2O_3)_2^{3-}$. The recovery remained consistent even when varying the concentration of $Au(S_2O_3)_2^{3-}$ in the presence of Mn^{2+} (Fig. S4). It could be concluded that the specific concentration dose not contribute to an enhanced effect of Mn^{2+}. There were two types of impurities, metal cations and $S_2O_3^{2-}$. Due to the negative charge of carbon electrodes [44], $S_2O_3^{2-}$ was repelled. Compared to metal cations, $Au(S_2O_3)_2^{3-}$ undergoes a reduction reaction at the electrode interface, leading to stronger adsorption than the electrostatic adsorption of metal ions onto the carbon electrode. Moreover, the pore size of the carbon electrode was more conductive to the adsorption and recovery of $Au(S_2O_3)_2^{3-}$. In summary, while impurities do have some impact on the reduction process, the main component being recovered is still $Au(S_2O_3)_2^{3-}$. Experimental evidence suggested that electro reduction-recovery can still have good recovery performances at the low gold(I) concentrations, even in the presence of impurity ions. For the application of this method in industry, this was a valuable discovery.

In the conditional experiments, a gold/thiosulfate molar ratio of 1:3 was employed. In general, the proportion of thiosulfate employed in industrial applications was larger, to ensure complete gold leaching. However, as the proportion of thiosulfate increased, the recovery deteriorated [45]. Consequently, excessive proportion of thiosulfate experiments had been conducted to assess the viability of the recovery effect. As shown in Fig. 6(b), although the recovery and reduction had decreased at high molar ratio, the reduction and recovery were not significantly affected, indicating a great potential application in thiosulfate leaching solutions. The findings of the experimental study demonstrated that this method had a broad range of applications.

With the aim of further applying the electro reduction-recovery method in factories, recovery experiments were also carried out on the actual leaching solutions (Fig. 7). Gold ores were obtained from

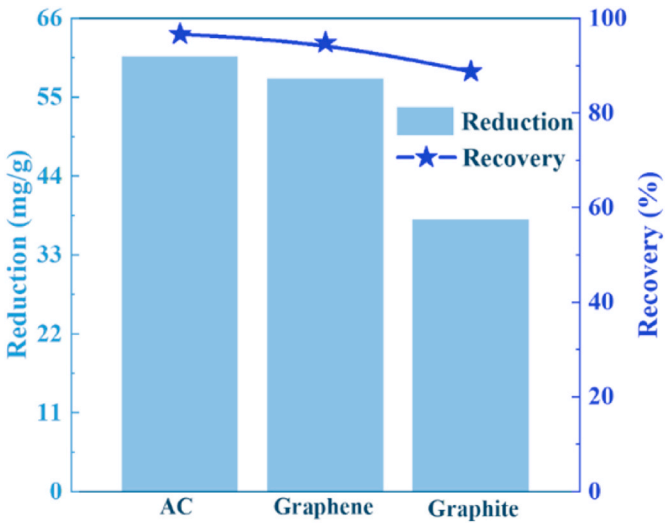

Fig. 7. Recovery performance of $Au(S_2O_3)_2^{3-}$ from gold thiosulfate leaching solutions via carbon electrodes.

factories, and then being leached by copper−sodium thiosulfate system. The recovery of $Au(S_2O_3)_2^{3-}$ achieved very high values, by AC and graphene electrodes, demonstrating the potential application of this method in real leaching solutions.

In order to ascertain the long-term stability of AC electrodes, this work also tested the recycling performance as shown in Fig. 8. The AC electrodes demonstrated good recyclability, however, after five cycles, the recovery decreased due to the material loss. This may be attributed to the poor adhesion of the material to the titanium plate.

3.5. Gold state on carbon electrodes

SEM and XPS were used to explore the gold state on the carbon material after being utilized as an electrode for $Au(S_2O_3)_2^{3-}$ recovery. SEM images (Fig. S5) exhibited similar morphology as before. Furthermore, XPS was carried out to investigate the state and interaction with $Au(S_2O_3)_2^{3-}$. Au element was observed on the carbon materials after Au $(S_2O_3)_2^{3-}$ recovery in the XPS survey spectrum (Fig. 9(a)), demonstrating that gold had been recovered successfully. To reveal the state of gold, the Au 4f XPS spectrum had been recorded and was shown in Fig. 9(d). The binding energy peaks of 83 and 87 eV corresponded to the $Au4f_{7/2}$ and $Au4f_{5/2}$ peaks, respectively, revealing the existence of the gold element (Au^0) after recovery. All the above results were evidences of the electro reduction-recovery of gold in the form of gold metal on the surface of the

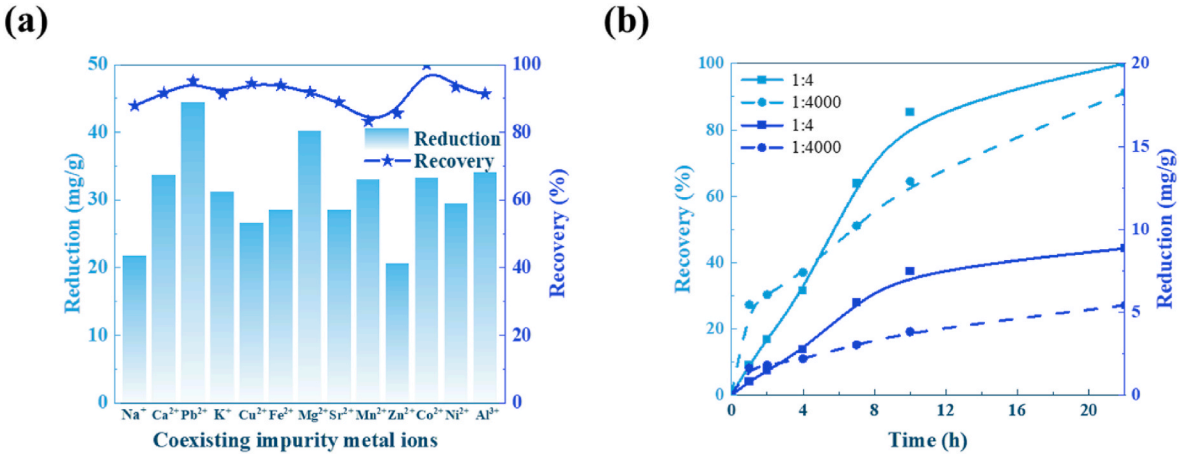

Fig. 6. $Au(S_2O_3)_2^{3-}$ recovery performances of AC electrodes under (a) inferred ions effects and (b) molar ratio of Au to $S_2O_3^{2-}$ effects.

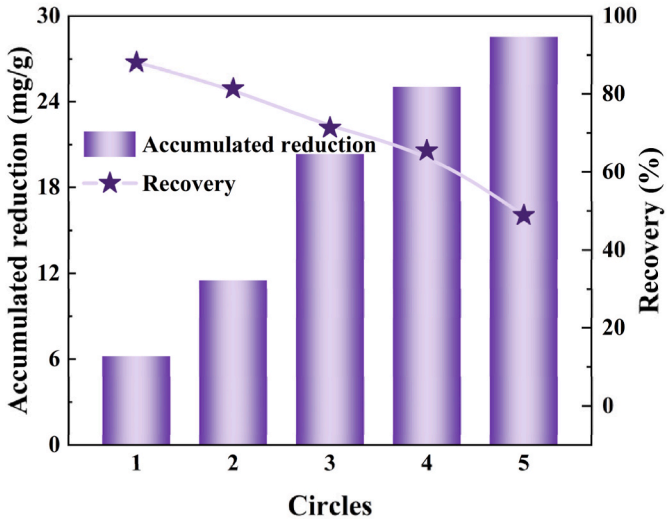

Fig. 8. The reusability of AC electrodes in $Au(S_2O_3)_2^{3-}$ recovery. (A colour version of this figure can be viewed online.)

carbon electrode.

The same functional groups as before the recovery were present in the spectra of the other elements, included C and O, as illustrated in Fig. 9(b and c). The C1s peak had undergone a shift towards a higher binding energy, exhibiting an approximate 0.7 eV increase compared to the pre-reaction state. This may be attributed to a change in the chemical valence state of carbon atoms during the recovery process, from a lower valence state (such as C–C or C–H) to a higher valence state (such as C═O or O–C═O), which resulted in an increase in electron binding energy [46,47]. An alternative hypothesis was that the adsorption of gold thiosulfate may result in a change in the electron density on the surface of the AC, thereby causing a shift in the C 1s peak. This change may be attributed to the formation of a chemical bond between Au $(S_2O_3)_2^{3-}$ and AC, such as the C–S bond between sulfur and carbon. The FTIR spectrum of carbon materials (Fig. S6) exhibited notable shifts in peak positions that many peaks have shown blue shifted, indicating alterations in the molecular structure or conformational changed upon interaction with the analyte. Decrease in some peaks intensity at certain wavenumbers suggested a reduction in the concentration of specific functional groups, such as AC at 2917–2850 and 1577 cm^{-1}. While the emergence of new peaks implied the formation of new bonds or the presence of additional chemical specie, S–H and C–S at 2515 and 713 cm^{-1} were the newly added peaks [48,49]. The electroreduction between the materials and the $Au(S_2O_3)_2^{3-}$ was mainly responsible for this. The adsorption of thiosulfate ions by the material resulted in a shift of the peak. Thiosulfate was a competitive ion [50,51], whereas carbon exerted an adsorption effect on $Au(S_2O_3)_2^{3-}$ [52].The broadening of peaks like O–H at 3430–3400 cm^{-1} may indicate increased molecular interactions or the presence of a distribution of similar but not identical vibrational modes. Substantially, these spectral modifications reflect the chemical and physical transformations occurring within the materials under investigation.

3.6. Electrochemical behaviors

To reveal the instinct electrochemical performances of $Au(S_2O_3)_2^{3-}$

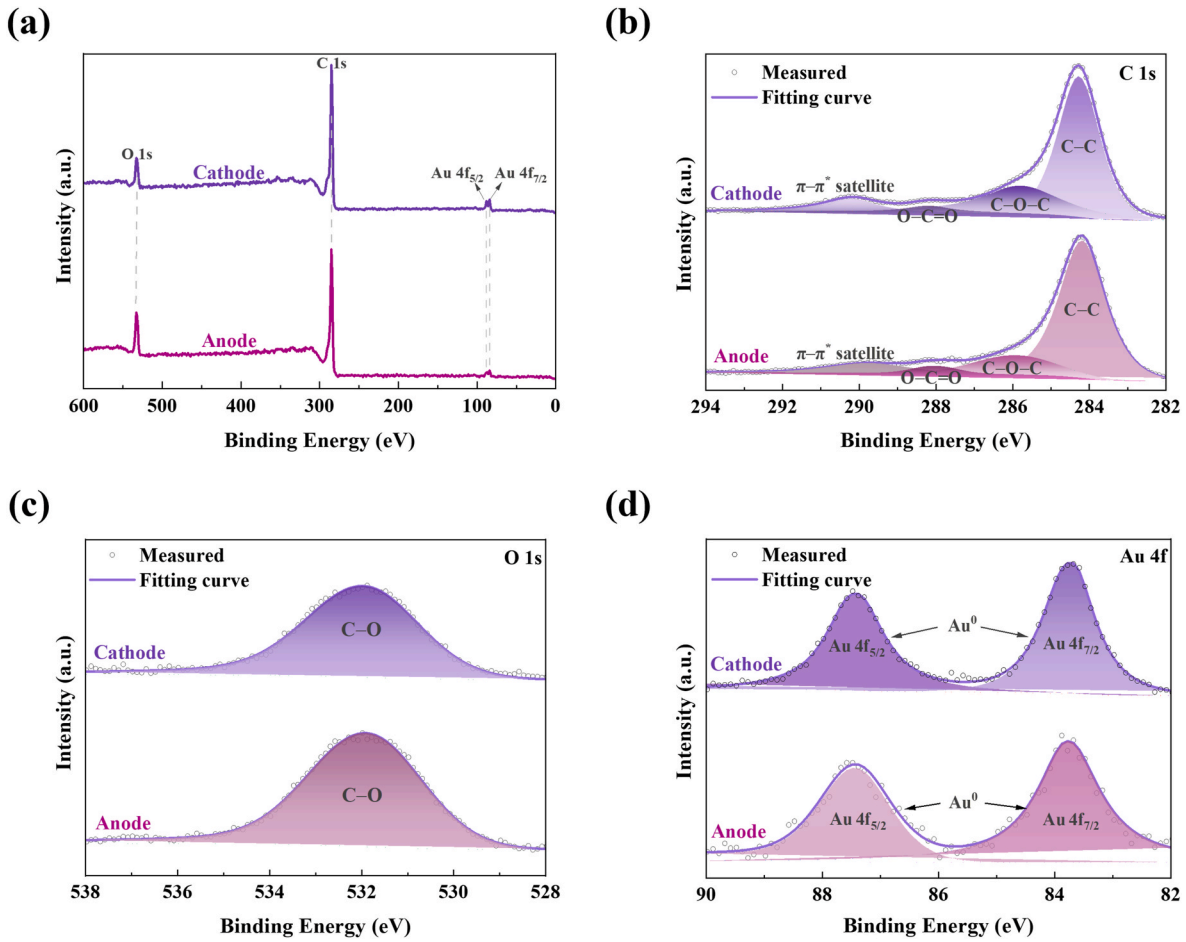

Fig. 9. (a) XPS survey spectra, (b) C 1s XPS spectra, (c) O 1s XPS spectra, and (d) Au 4f spectra of the AC electrode after $Au(S_2O_3)_2^{3-}$ recovery.

on carbon materials, CV and EIS were performed in Na_2SO_4 and Au $(S_2O_3)_2^{3-}$ solutions (Figure S7, S8 and Fig. 10). In EIS tests (Fig. 10 (a and c)), the AC electrode presented a semi-circle in the high frequency region, indicating the impedance of the charge transfer process. In contrast, no significant semicircle was observed for the graphite and graphene electrodes. This could be due to the electrochemical charge transfer reaction occurring very rapidly within the tested frequency range, highly active surface reaction kinetics resulting in minimal charge transfer impedance, or a highly uniform electrode surface with a high electrochemical reaction rate constant. In the high-frequency region, the impedance of the capacitor was lower, thus a significant response observed in this frequency range might indicate a larger capacitance value. The charge transfer resistance of alternating current is indicative of the speed and efficiency of electron transfer between the electrode and the electrolyte. A reduction in resistance facilitates the charge transfer process, thereby increasing the reaction rate and efficiency [53]. However, in our method, the double electric layer exerted a more pronounced influence, with the double electric layer being primarily associated with the pore and surface area [54]. After that, first to study electric double layer ability of carbon electrodes in Na_2SO_4 solution (Fig. S7), all CV curves did not display a substantial oxidation-reduction peak, denoting that the capacitances were predominantly provided by the double layer. Through the calculation (formula (3)), it was found that within the scanning speed range of 5–100 mV/s, AC had the highest specific capacitance, followed by graphene, and graphite demonstrated the lowest specific capacitance. Only AC exhibited a more obvious semicircle in the high-frequency region, indicating that it represented the highest resistance to charge transfer among the three materials and the slowest electron transfer kinetics.

To gain further insights into the reaction process, the CV curves in Au $(S_2O_3)_2^{3-}$ solutions (Fig. S8) revealed that in the $Au(S_2O_3)_2^{3-}$ solution, gold depletion occurred in the range of −0.2 to −0.8 V, which was indicative of a reduction reaction. Further calculations were conducted to ascertain the specific capacitance of the materials in $Au(S_2O_3)_2^{3-}$ as shown in Fig. 10(d). The results revealed that AC owned the highest specific capacitance, with graphene demonstrating a similar value. Nevertheless, the specific capacitance of graphite was relatively low in comparison to others, its recovery of $Au(S_2O_3)_2^{3-}$ was also poor. In terms of the order of intercept size, the sequence was as follows: graphene, AC, and graphite. It can be observed that an increase in the size of the intercept was accompanied by a proportional increase in the charge transfer resistance, which indicated that the charge transfer process was significantly impeded [55]. This suggested that graphene exhibited the most facile charge transfer process in accordance with the FTIR results, while graphite displayed the greatest impediment.

In charge transfer, the charge storage capacity of the materials, the electrochemical reaction's dynamic equilibrium, and the electric field activity in the electrolyte all affect the recovery process [56]. The electrochemical recovery efficiency can be significantly increased by the EDLC's exceptional charge storage capacity and effective charge transfer mechanism. EDLC may store a significant amount of charge by creating a double layer on the electrode surface. Additionally, choosing the right electrolyte can promote improved ion migration and storage, which will increase the recovery process's effectiveness [57].

In accordance with the present experiments, it could be posited that the recovery was contingent upon the electrochemical performance of

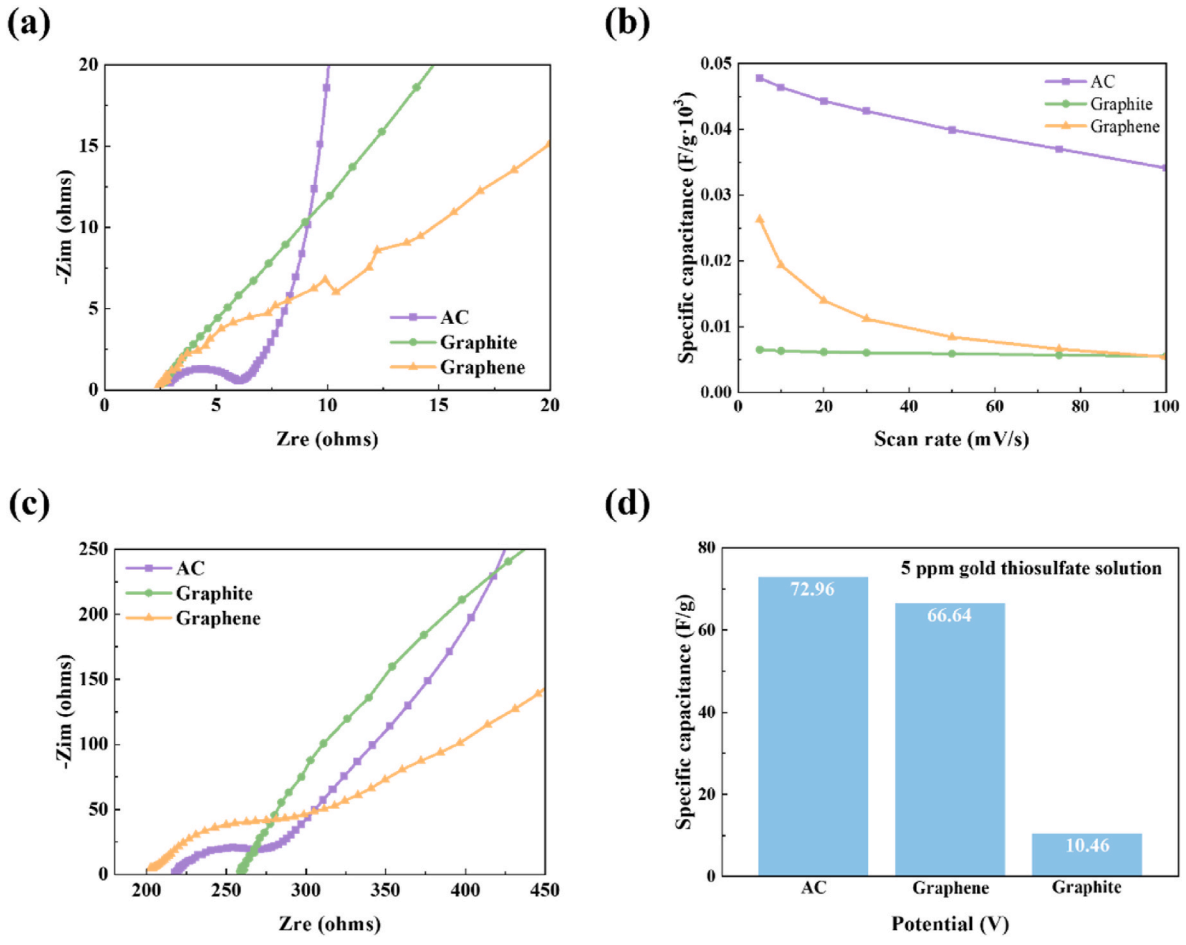

Fig. 10. (a) EIS curves, (b) specific capacitances of carbon electrodes in Na_2SO_4. (c) EIS curves, and (d) CV curves of carbon electrodes scanned at 1 mV s^{-1} in $Au(S_2O_3)_2^{3-}$.

the carbon materials. It can be demonstrated that an increase in the specific capacitance of the material would result in an enhanced recovery. The electrochemical performance of materials was correlated with their pore size and oxygen functional groups, whereby materials with a greater abundance of pores and oxygen functional groups exhibited a higher specific capacitance.

4. Conclusion

In this study, electro reduction-recovery of trace $Au(S_2O_3)_2^{3-}$ was proposed by the carbon electrodes. At an initial concentration of 1 mg/L, the recovery of $Au(S_2O_3)_2^{3-}$ achieved almost 100 %. Even in the presence of interfering ions (cations and $S_2O_3^{2-}$) and the actual thiosulfate leaching gold solutions, high recovery was obtained (higher than 90 %). Interestingly, $Au(S_2O_3)_2^{3-}$ was recovered in the form of gold metals, thus to shorten the traditional recovery and reduction procedures. It was found that the enhanced reduction and recovery abilities were relevant with electrochemical properties including EDLC and charge transfer. Higher EDLC improve the reduction capacity of $Au(S_2O_3)_2^{3-}$, which originated from richer pores and surface area. As for charge transfer ability, π–π* satellite was beneficial for charge migration, thereby enhancing reduction rate. This work gave a process to recover trace Au $(S_2O_3)_2^{3-}$ from thiosulfate leaching solutions using carbon electrodes and could be used on resources recycling. Since electrodeposition and electrode coating methods have been applied in gold recovery and battery technologies, there is significant potential for this approach to be utilized in industrial applications. However, addressing the issue of cycling stability is essential for promoting further research.

CRediT authorship contribution statement

Qizheng Weng: Writing – original draft, Investigation, Data curation. **Weiquan Zhan:** Writing – review & editing, Funding acquisition, Data curation. **Xuan Zhang:** Investigation. **Shaoxian Song:** Writing – review & editing, Funding acquisition. **Zhenlong Zeng:** Investigation. **Hnin May Lwin:** Data curation. **José Luis Arauz-Lara:** Data curation, Conceptualization. **Feifei Jia:** Supervision, Funding acquisition.

Declaration of competing interest

The authors declare that they have no known competing financial interests or personal relationships that could have appeared to influence the work reported in this paper.

Acknowledgements

This work was financially supported by the National Key Research and Development Program of China (No. 2021YFC2900900). Dr. Zhan gratefully acknowledges the Consejo Nacional de Humanidades Ciencias y Tecnologías (CONAHCYT) of Mexico for offering him the scholarship under the grant No. 813934 during his Ph.D. studies.

Appendix A. Supplementary data

Supplementary data to this article can be found online at https://doi.org/10.1016/j.carbon.2024.119799.

References

[1] H. Shang, Y. Chen, S. Guan, Y. Wang, J. Cao, X. Wang, H. Li, Z. Bian, Scalable and selective gold recovery from end-of-life electronics, Nat. Chem. Eng. 12 (1) (2024) 170–179, https://doi.org/10.1038/s44286-023-00026-w, 2024.
[2] D. Pattnaik, M.K. Hassan, A. Dsouza, A. Ashraf, Investment in gold: a bibliometric review and agenda for future research, Res. Int. Bus. Finance 64 (2023) 101854, https://doi.org/10.1016/J.RIBAF.2022.101854.
[3] A. Karppinen, S. Seisko, L. Nevatalo, B.P. Wilson, K. Yliniemi, M. Lundström, Gold recovery from cyanidation residue by chloride leaching and carbon adsorption – preliminary results from CICL process, Hydrometallurgy 226 (2024) 106304, https://doi.org/10.1016/J.HYDROMET.2024.106304.
[4] V.H. Ha, J. chun Lee, J. Jeong, H.T. Hai, M.K. Jha, Thiosulfate leaching of gold from waste mobile phones, J. Hazard Mater. 178 (2010) 1115–1119, https://doi.org/10.1016/J.JHAZMAT.2010.01.099.
[5] Z. wei Liu, X. yi Guo, Q. hua Tian, L. Zhang, A systematic review of gold extraction: fundamentals, advancements, and challenges toward alternative lixiviants, J. Hazard Mater. 440 (2022) 129778, https://doi.org/10.1016/J.JHAZMAT.2022.129778.
[6] X. Li, S. Chen, X. Hu, F. Zi, Efficient and selective recovery of gold from thiosulfate leaching solution using functionalized β-cyclodextrins synthesized by a steric hindrance strategy, Adv. Funct. Mater. 34 (2024) 2307472, https://doi.org/10.1002/ADFM.202307472.
[7] H. Qin, X. Guo, Q. Tian, D. Yu, L. Zhang, Recovery of gold from sulfide refractory gold ore: oxidation roasting pretreatment and gold extraction, Miner. Eng. 164 (2021) 106822, https://doi.org/10.1016/J.MINENG.2021.106822.
[8] L.M.M. Kinsman, B.T. Ngwenya, C.A. Morrison, J.B. Love, Tuneable separation of gold by selective precipitation using a simple and recyclable diamide, Nat. Commun. 121 (12) (2021) 1–8, https://doi.org/10.1038/s41467-021-26563-7, 2021.
[9] J. Kim, R. Kim, K.N. Han, Advances in hydrometallurgical gold recovery through cementation, adsorption, ion exchange and solvent extraction, Minerals 14 (2024), https://doi.org/10.3390/MIN14060607, 607. 14 (2024) 607.
[10] K. Fu, X. Liu, X. Zhang, S. Zhou, N. Zhu, Y. Pei, J. Luo, Utilizing cost-effective pyrocarbon for highly efficient gold retrieval from e-waste leachate, Nat. Commun. 151 (15) (2024) 1–13, https://doi.org/10.1038/s41467-024-50595-4, 2024.
[11] I. Korolev, S. Spathariotis, K. Yliniemi, B.P. Wilson, A.P. Abbott, M. Lundström, Mechanism of selective gold extraction from multi-metal chloride solutions by electrodeposition-redox replacement, Green Chem. 22 (2020) 3615–3625, https://doi.org/10.1039/D0GC00985G.
[12] A.F.M. Nogueira, A.R.F. Carreira, S.J.R. Vargas, H. Passos, N. Schaeffer, J.A. P. Coutinho, Simple gold recovery from e-waste leachate by selective precipitation using a quaternary ammonium salt, Sep. Purif. Technol. 316 (2023) 123797, https://doi.org/10.1016/J.SEPPUR.2023.123797.
[13] A. Yoshimura, M. Takai, Y. Matsuno, Novel process for recycling gold from secondary sources: leaching of gold by dimethyl sulfoxide solutions containing copper bromide and precipitation with water, Hydrometallurgy 149 (2014) 177–182, https://doi.org/10.1016/J.HYDROMET.2014.08.003.
[14] Z. Dong, T. Jiang, B. Xu, J. Wu, Q. Li, Y. Yang, A comparative study of electrodeposition and sodium dithionite reduction for recovering gold in gold-rich solution from the adsorption of thiosulfate solution by ion exchange resin, Sep. Purif. Technol. 328 (2024) 125053, https://doi.org/10.1016/J.SEPPUR.2023.125053.
[15] Z. Dong, T. Jiang, B. Xu, Q. Li, Y. Yang, Gold recovery from pregnant thiosulfate solution by ion exchange resin: synergistic desorption behaviors and mechanisms, Sep. Purif. Technol. 323 (2023) 124481, https://doi.org/10.1016/J.SEPPUR.2023.124481.
[16] W. Zhan, Y. Yuan, X. Yao, B. Yang, F. Jia, C. Lin, J.L. Arauz-Lara, S. Song, Efficient recovery of gold(I) from thiosulfate solutions through photocatalytic reduction with Mn(II)-Doped MoS2, ACS Sustain. Chem. Eng. 9 (2021) 11681–11690, https://doi.org/10.1021/ACSSUSCHEMENG.1C02160/ASSET/IMAGES/LARGE/SC1C02160_0012.JPEG.
[17] Y. Liang, W. Zhan, Y. Yuan, N. Zamora-Romero, F. Jia, B. Yang, Z. Nasrddinov, J. L. Arauz-Lara, S. Song, Manganese and oxygen dual-doping MoS2 boosts reduction and adsorption activity toward efficient recovery of gold(I) from thiosulfate solutions, J. Alloys Compd. 928 (2022) 167185, https://doi.org/10.1016/J.JALLCOM.2022.167185.
[18] J. Gao, W. Zhan, Z. Xiang, S. Song, J.L. Arauz-Lara, F. Jia, P. Chen, Facet engineering in cadmium sulfide for efficient reduction-recovery of low-concentration gold(I) from thiosulfate solutions, J. Mol. Liq. 413 (2024) 126018, https://doi.org/10.1016/J.MOLLIQ.2024.126018.
[19] W. Zhan, X. Zhang, Y. Yuan, Q. Weng, S. Song, M. de J. Martínez-López, J.L. Arauz-Lara, F. Jia, Regulating chemisorption and electrosorption activity for efficient uptake of rare earth elements in low concentration on oxygen-doped molybdenum disulfide, ACS Nano (2024), https://doi.org/10.1021/ACSNANO.4C00691.
[20] X. Zhang, W. Zhan, Q. Weng, S. Song, J. Luis Arauz-Lara, F. Jia, Electro-assisted sorption behavior and mechanism of low-concentration rare earth elements on carbon based materials, Appl. Surf. Sci. 664 (2024) 160224, https://doi.org/10.1016/J.APSUSC.2024.160224.
[21] F. Sun, Z. Li, H. Xu, Y. Fu, H. Li, Y. Yao, L. Ren, X. He, Y. Li, R. Yang, N. Zhang, Z. Hu, T. Ma, J. Zou, Exploring structural evolution behaviors of ligand-defect-rich ferrocene-based metal-organic frameworks for electrochemical oxygen evolution via operando X-ray absorption spectroscopy, Adv. Energy Mater. (2024) 2400875, https://doi.org/10.1002/AENM.202400875.
[22] S. Shivakumara, T.R. Penki, N. Munichandraiah, High specific surface area α-Fe2O3 nanostructures as high performance electrode material for supercapacitors, Mater. Lett. 131 (2014) 100–103, https://doi.org/10.1016/J.MATLET.2014.05.160.
[23] C.J. Weber, N.E. Strom, O. Simoska, Electrochemical deposition of gold nanoparticles on carbon ultramicroelectrode arrays, Nanoscale 16 (2024) 16204–16217, https://doi.org/10.1039/D4NR02326A.
[24] K. Tang, S. Yiacoumi, Y. Li, C. Tsouris, Enhanced water desalination by increasing the electroconductivity of carbon powders for high-performance flow-electrode capacitive deionization, ACS Sustain. Chem. Eng. 7 (2019) 1085–1094, https://doi.org/10.1021/ACSSUSCHEMENG.8B04746/ASSET/IMAGES/LARGE/SC-2018-04746C_0005.JPEG.

[25] T. Wang, Z. Zhang, Z. Gu, C. Hu, J. Qu, Electron transfer of activated carbon to anode excites and regulates desalination in flow electrode capacitive deionization, Environ. Sci. Technol. 57 (2023) 2566–2574, https://doi.org/10.1021/ACS.EST.2C09506/ASSET/IMAGES/LARGE/ES2C09506_0007.JPEG.
[26] J. Shui, F. Du, C. Xue, Q. Li, L. Dai, Vertically aligned N-doped coral-like carbon fiber arrays as efficient air electrodes for high-performance nonaqueous Li-O2 batteries, ACS Nano 8 (2014) 3015–3022, https://doi.org/10.1021/NN500327P/SUPPL_FILE/NN500327P_SI_001.PDF.
[27] S. Thangarasu, G. Palanisamy, S.H. Roh, H.Y. Jung, H.Y. Jung, H.Y. Jung, Nanoconfinement and interfacial effect of Pb nanoparticles into nanoporous carbon as a longer-lifespan negative electrode material for hybrid lead-carbon battery, ACS Sustain. Chem. Eng. 8 (2020) 8868–8879, https://doi.org/10.1021/ACSSUSCHEMENG.0C03461/ASSET/IMAGES/LARGE/SC0C03461_0008.JPEG.
[28] M. Chiku, H. Takeda, S. Matsumura, E. Higuchi, H. Inoue, Amorphous vanadium oxide/carbon composite positive electrode for rechargeable aluminum battery, ACS Appl. Mater. Interfaces 7 (2015) 24385–24389, https://doi.org/10.1021/ACSAMI.5B06420/ASSET/IMAGES/LARGE/AM-2015-06420X_0005.JPEG.
[29] M.N. Kleinberg, C. Thamaraiselvan, C.D. Powell, A. Ronen, C.J. Arnusch, Reduction of Cr(VI) to Cr(III) by activated carbon cloth through adsorption and electrochemical processes, ACS Appl. Eng. Mater. 1 (2023) 901–912, https://doi.org/10.1021/ACSAENM.2C00059.
[30] S. Gupta, A. Yadav, S. Singh, N. Verma, Synthesis of silicon carbide-derived carbon as an electrode of a microbial fuel cell and an adsorbent of aqueous Cr(VI), Ind. Eng. Chem. Res. 56 (2017) 1233–1244, https://doi.org/10.1021/ACS.IECR.6B03832/ASSET/IMAGES/LARGE/IE-2016-038323_0010.JPEG.
[31] M.A. Suliman, M. Sajid, M.K. Nazal, M.A. Islam, Carbon-based materials as promising sorbents for analytical sample preparation: recent advances and trends in extraction of toxic metal pollutants from various media, TrAC, Trends Anal. Chem. 167 (2023) 117265, https://doi.org/10.1016/J.TRAC.2023.117265.
[32] F.C. Vicentini, T.A. Silva, O. Fatibello-Filho, Carbon black electrodes applied in electroanalysis, Curr. Opin. Electrochem. 43 (2024) 101415, https://doi.org/10.1016/J.COELEC.2023.101415.
[33] L. Casanova, M. Gruarin, M.P. Pedeferri, M. Ormellese, A comparison between corrosion performances of titanium grade 2 and 7 in strong reducing acids, Mater. Corros. 72 (2021) 1506–1517, https://doi.org/10.1002/MACO.202112392.
[34] H.A.H. Abo Nama, İ. Esen, V. Karakurt, H. Ahlatci, Effect of the Ti addition on the corrosion behavior of newly developed AA7075-Ti alloys, J. Alloys Compd. 969 (2023) 172349, https://doi.org/10.1016/J.JALLCOM.2023.172349.
[35] M.R. Pantović Pavlović, B.P. Stanojević, M.M. Pavlović, M.D. Mihailović, J. S. Stevanović, V.V. Panić, N.L. Ignjatović, Anodizing/anaphoretic electrodeposition of nano-calcium phosphate/chitosan lactate multifunctional coatings on titanium with advanced corrosion resistance, bioactivity, and antibacterial properties, ACS Biomater. Sci. Eng. 7 (2021) 3088–3102, https://doi.org/10.1021/ACSBIOMATERIALS.1C00035/SUPPL_FILE/AB1C00035_SI_001.PDF.
[36] Y. Dou, Q. Bai, W. Guo, H. Wang, S. Chen, T. Wang, Study on the adsorption characteristics of organic contaminants on alumina surface coated with clean graphene and the influence of amorphous carbon on wetting behavior, Appl. Surf. Sci. 643 (2024) 158658, https://doi.org/10.1016/J.APSUSC.2023.158658.
[37] J. Park, S.S. Park, Y.S. Won, In situ XRD study of the structural changes of graphite anodes mixed with SiOx during lithium insertion and extraction in lithium ion batteries, Electrochim. Acta 107 (2013) 467–472, https://doi.org/10.1016/J.ELECTACTA.2013.06.059.
[38] B. Tang, L. Zheng, X. Dai, H. Chen, Nitrogen/oxygen co-doped porous carbons derived from a facilely-synthesized Schiff-base polymer for high-performance supercapacitor, J. Energy Storage 26 (2019) 100961, https://doi.org/10.1016/j.est.2019.100961.
[39] D. Chen, K. Cen, X. Zhuang, Z. Gan, J. Zhou, Y. Zhang, H. Zhang, Insight into biomass pyrolysis mechanism based on cellulose, hemicellulose, and lignin: evolution of volatiles and kinetics, elucidation of reaction pathways, and characterization of gas, biochar and bio-oil, Combust. Flame 242 (2022) 112142, https://doi.org/10.1016/J.COMBUSTFLAME.2022.112142.
[40] Z. Luo, B. Yao, X. Yang, L. Wang, Z. Xu, X. Yan, L. Tian, H. Zhou, Y. Zhou, Novel insights into the adsorption of organic contaminants by biochar: a review, Chemosphere 287 (2022) 132113, https://doi.org/10.1016/J.CHEMOSPHERE.2021.132113.
[41] S. Iftekhar, D.L. Ramasamy, V. Srivastava, M.B. Asif, M. Sillanpää, Understanding the factors affecting the adsorption of Lanthanum using different adsorbents: a critical review, Chemosphere 204 (2018) 413–430, https://doi.org/10.1016/J.CHEMOSPHERE.2018.04.053.
[42] W. Zhan, Y. Yuan, B. Yang, F. Jia, S. Song, Construction of MoS2 nano-heterojunction via ZnS doping for enhancing in-situ photocatalytic reduction of gold thiosulfate complex, Chem. Eng. J. 394 (2020) 124866, https://doi.org/10.1016/j.cej.2020.124866.
[43] Y.A. Peng Zhou, Gang Xin, Changgong Meng, Jian Xin, Huilong Wang, Yongxian Yu, Wensheng Mou, Inorganic Chemistry, fifth ed., Higher Education Press, Beijing, 2006.
[44] X. Zhang, W. Zhan, Q. Weng, S. Wang, S. Song, J.L. Arauz-Lara, F. Jia, Electro reduction-recovery of Au(S2O3)23– within a low concentration range via multi-porous activated carbon electrodes, Sep. Purif. Technol. 354 (2024) 129134, https://doi.org/10.1016/J.SEPPUR.2024.129134.
[45] K. Sun, S. Mao, W. Zhan, C. Liu, F. Jia, S. Song, In-situ reduction of Au(S2O3)23− for efficient recovery of gold with magnetically separable shell-core structured MoS2@Fe3O4 composite, Hydrometallurgy 198 (2020), https://doi.org/10.1016/J.HYDROMET.2020.105514.
[46] L.M. Haselbach, S. Ma, Potential for carbon adsorption on concrete: surface XPS analyses, Environ. Sci. Technol. 42 (2008) 5329–5334, https://doi.org/10.1021/ES800717Q/ASSET/IMAGES/ES-2008-00717Q_M005.GIF.
[47] Y.C. Wang, M.H. Engelhard, D.R. Baer, D.G. Castner, Quantifying the impact of nanoparticle coatings and nonuniformities on XPS analysis: gold/silver core-shell nanoparticles, Anal. Chem. 88 (2016) 3917–3925, https://doi.org/10.1021/ACS.ANALCHEM.6B00100/ASSET/IMAGES/LARGE/AC-2016-00100A_0008.JPEG.
[48] M. Yin, X. Bai, D. Wu, F. Li, K. Jiang, N. Ma, Z. Chen, X. Zhang, L. Fang, Sulfur-functional group tunning on biochar through sodium thiosulfate modified molten salt process for efficient heavy metal adsorption, Chem. Eng. J. 433 (2022) 134441, https://doi.org/10.1016/J.CEJ.2021.134441.
[49] H. Klym, I. Karbovnyk, M.C. Guidi, O. Hotra, A.I. Popov, Optical and vibrational spectra of CsCl-enriched GeS2-Ga2S3Glasses, Nanoscale Res. Lett. 11 (2016) 1–6, https://doi.org/10.1186/S11671-016-1350-8/FIGURES/3.
[50] S. Cherevko, A.A. Topalov, A.R. Zeradjanin, I. Katsounaros, K.J.J. Mayrhofer, Gold dissolution: towards understanding of noble metal corrosion, RSC Adv. 3 (2013) 16516–16527, https://doi.org/10.1039/C3RA42684J.
[51] J.R. Reimers, M.J. Ford, S.M. Marcuccio, J. Ulstrup, N.S. Hush, Competition of van der Waals and chemical forces on gold–sulfur surfaces and nanoparticles, Nat. Rev. Chem 12 (1) (2017) 1–13, https://doi.org/10.1038/s41570-017-0017, 2017.
[52] M. Soleymani, F. Sadri, S. Zhang, A. Ghahreman, The role of thiosulfate and sulfite in gold thiosulfate electrowinning process: an electrochemical view, Process Saf. Environ. Protect. 166 (2022) 232–240, https://doi.org/10.1016/J.PSEP.2022.08.028.
[53] Z. Tang, Q.A. Huang, Y.J. Wang, F. Zhang, W. Li, A. Li, L. Zhang, J. Zhang, Recent progress in the use of electrochemical impedance spectroscopy for the measurement, monitoring, diagnosis and optimization of proton exchange membrane fuel cell performance, J. Power Sources 468 (2020) 228361, https://doi.org/10.1016/J.JPOWSOUR.2020.228361.
[54] Y. Zhu, H. Shen, I. Zada, H. Li, Y. Li, S. Zhu, Y. Li, Surface engineering of porous carbons for next-generation supercapacitors, J. Energy Storage 100 (2024) 113608, https://doi.org/10.1016/J.EST.2024.113608.
[55] H.S. Magar, R.Y.A. Hassan, A. Mulchandani, Electrochemical impedance spectroscopy (Eis): principles, construction, and biosensing applications, Sensors 21 (2021), https://doi.org/10.3390/S21196578.
[56] P. Srimuk, X. Su, J. Yoon, D. Aurbach, V. Presser, Charge-transfer materials for electrochemical water desalination, ion separation and the recovery of elements, Nat. Rev. Mater. 57 (5) (2020) 517–538, https://doi.org/10.1038/s41578-020-0193-1, 2020.
[57] S. Dong, Z. Li, Z. Yi, H. Li, Y. Tian, S. Liu, Recycling of activated carbons from spent supercapacitors to refabricate improved supercapacitors, J. Energy Storage 102 (2024) 114182, https://doi.org/10.1016/J.EST.2024.114182.